Solketal synthesis from ketalization of glycerol with acetone: A kinetic study over a sulfated zirconia catalyst

Julián A. Vannucci, Nora N. Nichio, Francisco Pompeo

PII: S0920-5861(20)30678-7

DOI: https://doi.org/10.1016/j.cattod.2020.10.005

Reference: CATTOD 13158

To appear in: *Catalysis Today*

Received Date: 18 May 2020

Revised Date: 19 August 2020

Accepted Date: 1 October 2020

Please cite this article as: Vannucci JA, Nichio NN, Pompeo F, Solketal synthesis from ketalization of glycerol with acetone: A kinetic study over a sulfated zirconia catalyst, *Catalysis Today* (2020), doi: https://doi.org/10.1016/j.cattod.2020.10.005

Solketal synthesis from ketalization of glycerol with acetone: A kinetic study over a sulfated zirconia catalyst

Julián A. Vannucci[a,b], Nora N. Nichio[a,b], Francisco Pompeo[a,b,*]

[a] Centro de Investigación y Desarrollo en Ciencias Aplicadas (CINDECA), Facultad de Ciencias Exactas, Universidad Nacional de La Plata (UNLP) – CONICET, Calle 47, 257, CP 1900, La Plata, Argentina.

[b] Facultad de Ingeniería, Universidad Nacional de La Plata (UNLP), Calle 1 esq. 47, CP 1900, La Plata, Argentina.

*fpompeo@quimica.unlp.edu.ar (Francisco Pompeo)

Graphical abstract

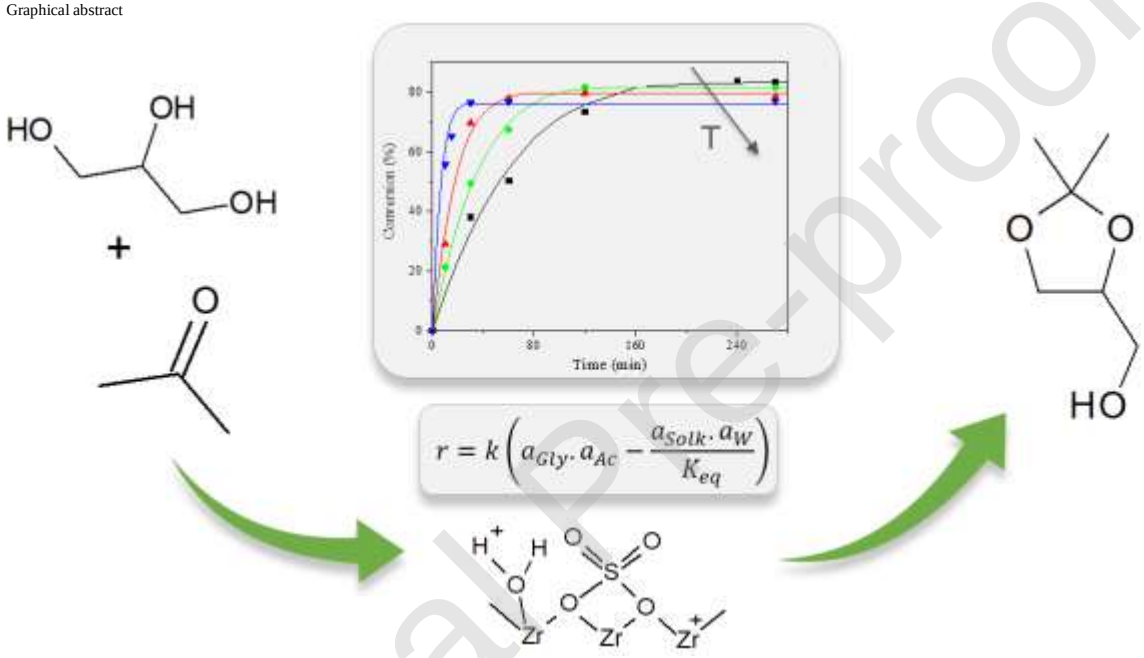

Highlights

- SO_4/ZrO_2 were prepared by a simple wet impregnation technique.
- A simple pseudo-homogeneous kinetic expression was developed and validated.
- The activation energy of the reaction was estimated as 88.1 ± 8.9 kJ/mol.
- Water largely affects the reaction rate and the conversion at equilibrium state.

Abstract

In this work, a series of acid catalysts were synthetized from a commercial zirconium oxide sulfated with a 0.5 M H_2SO_4 solution by wet impregnation. The characterization results show a correlation between the calcination temperature and the acid sites generated on the

materials. Among the catalysts prepared, the sulfated zirconia calcined in air at 400 °C (Zr-S-400), with a molar ratio S/Zr = 0.23 was the most active one due to its larger acid density and greater acid strength caused by the generation of new Brönsted sites. The Zr-S-400 catalyst exhibited an initial reaction rate of 0.0497 $mol.min^{-1}.g^{-1}$, and achieved a glycerol conversion of 80% in 1 hour of reaction at 40°C (glycerol:acetone molar ratio =1:6). The Zr-S-400 material remained stable after four catalytic cycles, demonstrating the stability of the superficial sulfate species (S/Zr ~ 0.2). In addition, the thermodynamics and kinetics of the reaction were evaluated, as well as the influence of some operating conditions such as the molar ratio of reactants and the water content in the reaction mixture. The following standard molar reaction properties were obtained: ΔH^o = -11.6 ± 1.1 $kJ.mol^{-1}$ and ΔG^o = 4.0 ± 0.1 $kJ.mol^{-1}$. Taking into account that the adsorption of water on this catalyst did not affect the number of acid sites available, a simple pseudo-homogeneous kinetic expression was developed and successfully adjusted to the experimental data in the range under study. Based on this model, the estimated activation energy of the reaction was 88.1 ± 8.9 $kJ.mol^{-1}$.

Keywords: Solketal, Sulfated zirconia, Batch reactor, Kinetic model.

1. Introduction

Glycerol is a promising biomass platform molecule having several applications in many industries. Nowadays, the development of new technological ways to add value to glycerol has become a research hotspot. Many studies have focused on the valorization of glycerol through catalytic processes such as ketalization, dehydration, oxidation, and reforming. In particular, the condensation reaction of glycerol with carbonyl compounds to produce oxygenated compounds has received great attention [1]. Among the different glycerol ketals, solketal is highly valuable for its potential applications as a green solvent, plasticizer in the polymer industry [2], and solubilizing and suspending agent in biodegradable systems for the controlled release of medicinally active substances [3]. In addition, it can be used as a fuel additive to increase the octane number and reduce gum formation [4]. Solketal is normally synthesized by the ketalization of glycerol with acetone (Scheme 1).

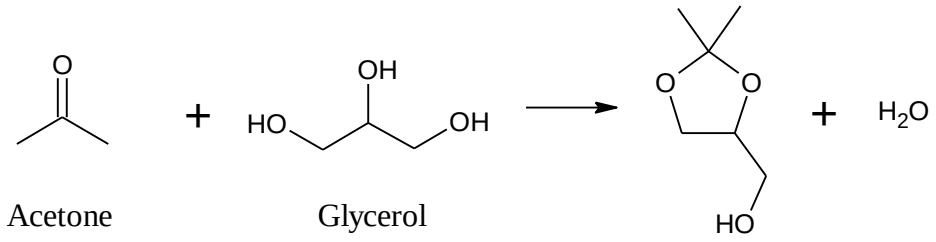

Acetone Glycerol Solketal

Scheme 1: Ketalization of glycerol with acetone

The miscibility of both reactants, glycerol and acetone, is poor. However, as the reaction progresses, the produced solketal acts as a cosolvent, improving the solubility of glycerol in the acetone phase [5]. Thus, an excess of acetone is often used as a solubility enhancer [5] and to shift the chemical equilibrium toward the formation of solketal [2]. Despite these problems, several reports have shown that the reaction could be successfully carried out with heterogeneous catalysts such as ion exchange resins [6], heteropolyacids [7], acid clays [8], mesostructured silicas [9-11], and zeolites [12-14]. In comparison to the aforesaid catalysts, promoted metal oxides offer several advantages, since they are stable, regenerable, and active. Li et al. synthesized layered crystalline α-zirconium phosphates and studied the effect of the calcination temperature over the acid properties of the material. The results showed that materials with a relation P/Zr ~ 2 possess higher surface density of acid sites and stability when calcined at temperatures below 300°C. The conversion of glycerol decreased from 86 to 45% with the increasing calcination temperature from 200 to 600ºC, which was attributed to the decomposition of the active species $Zr(HPO_4)_2 \cdot H_2O$ to ZrP_2O_7 [15].

Miao et al. synthesized a series of ordered mesoporous titanium phosphate (M-TiPO) materials with controllable composition by a simple one-pot method. With the incorporation of highly dispersed P species in the structure of M-TiPO, the bonds in the material transferred from Ti-O-Ti to Ti-O-P bonds, thus improving the acid properties of the material. The M-TiPO catalyst with a P/Ti ratio = 0.75 exhibited the best catalytic effect, achieving a glycerol conversion of 91% and a selectivity to solketal of 94% [16].

Recently, Li et al. prepared a series of zirconium organophosphates with different quantities of fenil groups following a hydrothermal method. The materials showed a hydrophobic

character which was enhanced with an increasing amount of phenyl groups. The best activity was attributed to both abundant acidity and optimal hydrophilia/hydrophobicity balance [17].

In reactions requiring acid materials, sulfate species represent one of the most widely used promoters of metal oxides [18,19]. The sulfated zirconia catalyst has been employed in many industrially important vapor-phase reactions such as dehydration of ethanol [20], alkylation of isobutane with 2-butene [21], and isomerization of hydrocarbons [22-24]. Furthermore, it has been found to be very active in liquid-phase reactions, such as Friedel-Crafts monoalkylation [18], synthesis of aromatics gem-dihalides [25], stereocontrolled glycosidation [26], etc.

The application of sulfated zirconia to the ketalization of glycerol with acetone has been previously explored [27-29]. Reddy et al. compared diverse promoters of zirconia, such as W, Mo, and sulfate ions, concluding that the sulfated promoted zirconia showed the highest catalytic activity due to its higher surface area and number of acidic sites. Although their study demonstrated the efficacy of sulfated zirconia in glycerol ketalization, the stability of the catalyst and the kinetics of the reaction were not evaluated [27].

Nanda et al. compared a zirconium sulfate catalyst in the synthesis of solketal in a continuous flow reactor with different commercial materials. According to the yield to solketal and glycerol conversion, the activity of these catalysts followed the sequence Amberlyst Wet ~ Zeolite ~ Amberlyst Dry > Zirconium Sulfate > Montmorillonite > Polymax. The stability of these catalysts was analyzed and a slight decrease in the activity was found, likely due to the loss of its acidity after a long time on stream [29].

The objectives of this work were to develop an efficient catalyst for the synthesis of solketal and determine the thermodynamic and kinetic parameters, which are essential tools for understanding the reactive system, designing reactors, and scaling up the process. For this purpose, commercial ZrO_2 was promoted with H_2SO_4 following a wet impregnation technique and employed as a catalyst to carry out the ketalization of glycerol with acetone. Once the catalyst was proven efficient and stable, several experimental data were collected in order to determine a kinetic expression that describes the reaction behavior accurately. Characterization techniques, such as XRD, N_2 adsorption-desorption, potentiometric

titration, XPS, and Pyridine FTIR, were employed to relate the catalytic activity results to the presence of acid sites.

2. Experimental

2.1. Materials

Glycerol (99.5%), absolute ethanol (99.5%) and sulfuric acid (98%) were purchased from Cicarelli. Acetone (99.5%), n-propanol (99.3%), and acetonitrile (99.8%) were purchased from Anedra. Solketal (98.2%) was purchased from TCI Chemicals, and powder zirconium oxide was purchased from MEL Chemicals.

2.2. Catalyst preparation

A commercial zirconium oxide powder, namely Zr, was subjected to a thermal treatment at 600 °C for 5 hours, resulting in sample Zr_{600}. Both materials, Zr and Zr_{600}, were promoted with a proper amount of 0.5M H_2SO_4 solution, following a wet impregnation technique. Excess water was evaporated on a water-bath at 60 °C assisted by ultrasound, oven-dried, and calcined in air at 400 (Zr-S-400, Zr_{600}-S-400) and 600 °C (Zr-S-600) for 5 hours.

2.3. Catalyst characterization

The XRD patterns in the 2θ angular range from 10 to 70° were obtained with a Philips 3710 X'Pert using CuKα radiation, with a 0.04°/min step. The identification of the XRD phases present in the sample was aided by JCPDS data files.

Textural properties were determined by nitrogen adsorption-desorption isotherms at the temperature of liquid nitrogen (-196°C) in a Micrometrics ASAP 2020 instrument. Before adsorption, the samples were evacuated by heating at 100 °C in vacuum, with a pressure lower than 4 Pa for 12 hours. The specific surface area was calculated according to the Brunauer-Emmett-Teller (BET) equation, in the relative pressure range 0.05-0.35 [30]. The pore size distribution was obtained by the Barret-Joyner-Halenda (BJH) method, using the adsorption branch and assuming slit-shape pore geometry [31].

The X-ray photoelectron spectroscopy (XPS) measurements were performed using a non-monochromatic Al Kα source (XR50, Specs GmbH) and a hemispherical electron energy

analyzer (PHOIBOS 100, Specs GmbH). O 1s, Zr 3d, S 2p, and C 1s lines were monitored. C 1s at 284.6 eV was used as a charging reference. Spectra were analyzed with CasaXPS software.

The amount and strength of acid sites were estimated by potentiometric titration. A known mass (0.05 g) of the solids was suspended in acetonitrile and kept under stirring for 3 hours. The suspension was titrated with a solution of n-butylamine in acetonitrile (0.05 M) at 0.05 ml min^{-1}. The electrode potential variation was obtained on a digital pH meter (Metrohm 794 Basic Titrino apparatus with a double junction electrode).

Pyridine FTIR was used to characterize the nature of the acid sites. Spectra were recorded with a Thermo Nicolet iS10. To create a clean surface for the analysis, the catalysts were heated to 400 °C under vacuum conditions and maintained for 1 hour. Thereafter, the catalyst was cooled to room temperature to collect the background spectra from the clean surface. After background collection, the adsorption was performed on the cell at 25 °C. The excess pyridine was desorbed with a vacuum from room temperature to 400 °C with 100 °C steps. Brönsted and Lewis acid quantification was performed from 1545 cm^{-1} and 1450-1460 cm^{-1} bands, respectively, using the literature data on the integrated molar extinction coefficients [32].

2.4. Catalytic activity measurements

The ketalization of glycerol was carried out in a 200 ml Büchi glass batch reactor equipped with a manometer, magnetic stirrer, thermostatic bath, gas inlet, and release valves. Before the catalytic evaluation, experiments were performed to verify the negligible contribution of the reaction in the absence of a catalyst and in the absence of external and internal diffusion limitations.

In a typical experiment, acetone, glycerol, and the catalyst are loaded in a reactor. Then, the reactor is pressurized to 0.2 MPa with N_2 and heated to the desired temperature. As previously mentioned, the use of an excess of acetone improves the amount of solubilized glycerol. Molar ratios of glycerol to acetone in the range of 1:2 to 1:20 have been reported in the literature [33]. However, molar ratios greater than 1:10 do not generate significant impact on catalytic performance [34-36]. Concerning the catalyst, mass values between 0.5% and 5% wt. related to glycerol are commonly used [6, 8, 27, 37, 38]. In our

experiments, we employed a catalyst amount in the range of 0.3% to 2.5% wt. of the total mass of glycerol and molar ratios glycerol:acetone in the range of 1:4 to 1:8.

Once the experiment was over, the reactor was cooled to 20 °C and the catalyst was separated by centrifugation and filtration. The reactants and products were analyzed by gas chromatography with a Shimadzu GCMS-QP505A, equipped with a PE-Elite-Wax capillary column, and an FID detector, using n-propanol as an external standard.

The conversion was determined with the following equation:

$$X\% = \frac{(initial\ glycerol\ moles - final\ glycerol\ moles)}{initial\ glycerol\ moles}$$

and the selectivity to solketal with

$$S\% = \frac{solketal\ moles}{(initial\ glycerol\ moles - final\ glycerol\ moles)}$$

2.5. Thermodynamic and Kinetic studies

The equilibrium thermodynamic constant, K_{eq}, can be determined by the following equation

$$K_{eq} = \frac{a_{Solk}.a_W}{a_{Gly}.a_{Ac}} \quad (1)$$

$$a_i = \gamma_i.x_i \quad (2)$$

The activity coefficients (γ_i) at different temperatures and compositions were calculated by UNIFAC [39] with the groups listed in Table S1 (Supplementary Information).

The reaction mechanism proposed in the literature [40-42] is represented in Scheme 2. In the first step, glycerol and acetone interact forming a hemiketal (3-(2-hydroxypropan-2-yloxy)propane-1,2-diol) [40]. The second step differs depending on whether the reaction is conducted under Brönsted acid sites or Lewis acid sites. In the presence of Brönsted acid sites, a carbenium ion is stabilized and activated for a nucleophilic attack from one of the alcoholic groups of glycerol, leading to the formation of solketal or the six-membered ring ketal (2,2-dimethyl-1,3-dioxan-5-ol) [41]. The presence of Lewis acid sites coordinates and activates the tertiary alcohol of the hemiketal. Then, an intramolecular reaction with one of the alcoholic groups leads to the formation of solketal and the isomer [42].

Although both solketal and 2,2-dimethyl-1,3-dioxan-5-ol isomer are produced in the reaction, selectivities toward solketal higher than 80% have been reported by several authors. This could be related to the presence of a methyl group in the axial position of the six-membered ring of 2,2-dimethyl-1,3-dioxan-5-ol, making this molecule less thermodynamically stable than the solketal molecule [43].

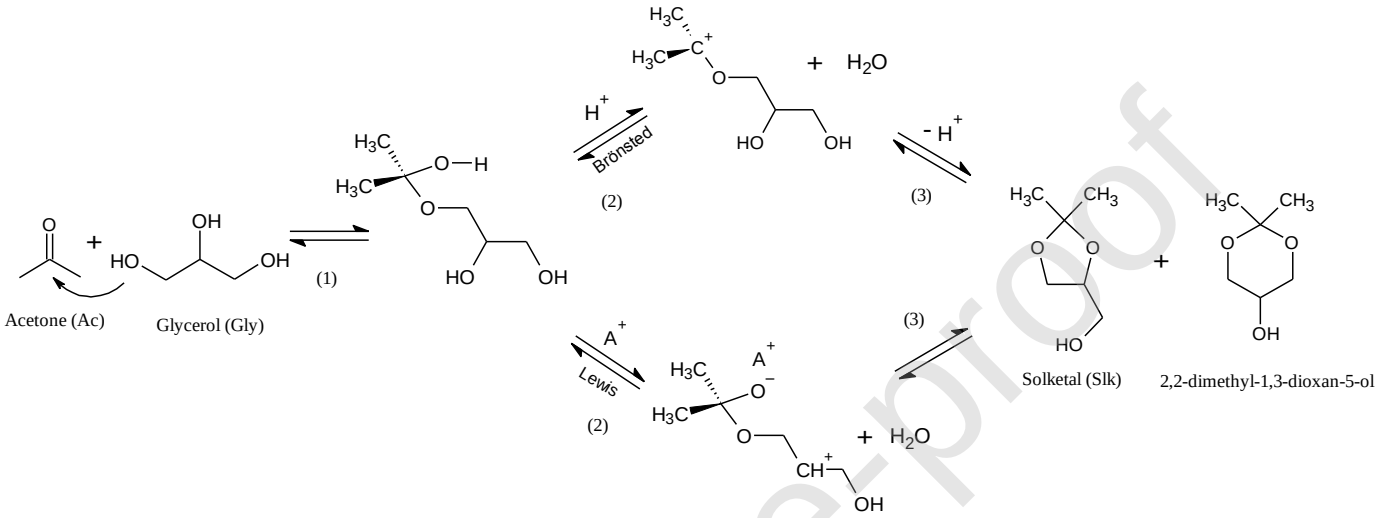

Scheme 2: Reaction mechanism proposed for the ketalization of glycerol with acetone over acid catalysts (adapted from Calvino-Casilda et al. [40]).

The reaction rate of the glycerol ketalization could be expressed in the form of a Langmuir-Hinshelwood-Hougen-Watson (LHHW) model [44,45]. The mechanism is based on the adsorption of both reactants (glycerol and acetone) on the catalyst surface, followed by three consecutive reactions (Scheme 2) and the desorption of the products (water and solketal).

The kinetic parameters were estimated by implementing the Orthogonal Distance Regression algorithm for nonlinear curve fitting using OriginLab software. The differences between the predicted values for the variation of the glycerol concentration over time and the experimental data were minimized using the chi-squared criterion.

The Mears criterion and Weisz-Prater criterion were used to evaluate external and internal diffusion limitations. For this purpose, the diffusivity coefficients for each component, the diffusivity coefficient of the multicomponent system, and the mass transfer coefficient were estimated with the Scheibel correlation [46], Perkins and Geankoplis correlation [47] and the Hixson and Baum correlation [48], respectively.

3. Results and discussion

3.1. Catalytic Activity

Since the ketalization of glycerol with acetone requires the presence of strong acid sites, this reaction represents an additional characterization technique to evidence these active sites. The non-promoted materials, samples Zr and Zr_{600}, were not active in this reaction, which shows their lack of strong acid sites. By contrast, all sulfated samples were active in the reaction. Table 1 presents the initial reaction rate and selectivities for each catalyst. (determined in the first 10 minutes of the reaction). In all reactions, only solketal and 2,2-dimethyl-1,3-dioxan-5-ol were identified as reaction products. Some authors have reported the presence of subproducts such as 4-hydroxy-4-methyl-2-pentanone [49], 1,2,3-propanetriol monoacetate, 2-(1-hydroxypropan-2-yloxy)-propane-1,2-diol and 3-(1-hydroxypropan-2-yloxy)-propane-1,2-diol [50 - 52], in the presence of a catalyst with redox properties such as Nb [49], Co, Ni, or Pt [50, 51]. Therefore, the absence of these properties in our catalyst improves the selectivity toward solketal. These results show that the pre-calcined and sulfated Zr_{600}-S-400 sample presents two-thirds of the catalytic activity in comparison with sample Zr-S-400. In addition, sample Zr-S-600 was the least active. The characterization of the results presented in Section 3.2 shows the relationship between this catalytic behavior and the acidic and textural properties of the sample.

Table 1: Initial reaction rate. Experimental conditions: 10 min reaction, 40 °C; 0.2 MPa N_2, glycerol: acetone molar ratio = 1:6, 0.6 wt.% (catalyst:glycerol).

Sample	Initial reaction rate ($mol.min^{-1}.g^{-1}$)	$S_{Solketal}$ (%)	$S_{2,2\text{-dimethyl-1,3-dioxan-5-ol}}$ (%)
Zr-S-400	0.0497	86	14
Zr-S-600	0.0217	88	12
Zr_{600}-S-400	0.0361	81	19

Sample Zr-S-400 was the most active and it was, therefore, selected for the kinetic study. The study of the stability of the Zr-S-400 catalyst represents an important factor in every kinetic determination. For this purpose, four activity cycles of the same catalyst batch were performed. After each run, the reaction mixture was separated from the catalyst by centrifugation and filtration, and the catalyst was reintroduced into the reactor (without any treatment). After these four runs (Figure 1), the catalyst showed a 16% decrease over its initial activity. Since the separation process could lead to small losses of fine catalyst powders, the result obtained in this study is remarkable, evidencing the stability of the material. From these results, a kinetic study of the ketalization of glycerol with an acetone reaction was performed using the Zr-S-400 catalyst.

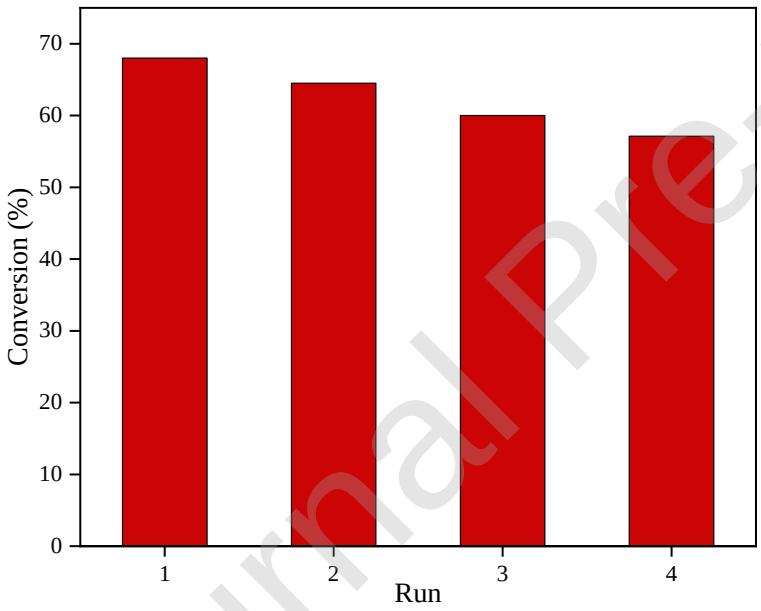

Figure 1: Stability of Zr-S-400. Experimental conditions: 40 °C; 0.2 MPa N_2, glycerol:acetone molar ratio = 1:6, 0.3 wt.% (catalyst: glycerol) and an 80 min reaction in each run.

3.2. Superficial characterization

The N_2 adsorption-desorption isotherms obtained for the samples are shown in the Supplementary Information (Figure S1). All samples show type IV isotherms with a hysteresis loop of H3 type according to the IUPAC classification. Table 2 summarizes the values of specific areas, average pore size, and total pore volume, for all the samples prepared.

Table 2: Textural and acidic properties

	BET			Potentiometric titration	
Sample	BET Surface ($m^2.g^{-1}$)	Pore volume ($cm^3.g^{-1}$)	Pore diameter (nm)	E_0 (mV)	meq n-butylamine.g^{-1}
Zr	105	0.34	5.1	63	0.20
Zr_{600}	49	0.30	12.3	134	0.15
Zr-S-400	58	0.23	5.8	560	0.75
Zr-S-600	86	0.29	5.9	310	0.52
Zr_{600}-S-400	24	0.13	11	510	0.52

Figure 2 presents the XRD patterns of commercial zirconia and sulfate promoted zirconium oxides. It can be observed that all materials exhibit both characteristic peaks from the monoclinic (2θ = 28.19°, 31.48°, 34.17°, 50.13°) and tetragonal zirconia phase (2θ = 30.18°), the monoclinic phase being dominant (JCPDS 86-1451, JCPDS 81-1544). Given that all diffractograms show the same characteristic peaks, it is possible to conclude that sulfation and subsequent heat treatment do not substantially modify the crystal structure. However, some morphological changes are evidenced. Calcination of the commercial

zirconium oxide at 600 °C (sample Zr_{600}) results in a drop in surface area and, therefore, an increase in the pore diameter from 5.1 to 12.3 nm.

Regarding the sulfated samples, Zr-S-400 and Zr_{600}-S-400 present smaller surface areas than the unsulfated oxides, which would indicate the incorporation of sulfated species. By contrast, the larger surface area of the sulfated sample Zr-S-600 in comparison to sample Zr-S-400 could be evidence of the loss of sulfate groups caused by an increase in the calcination temperature.

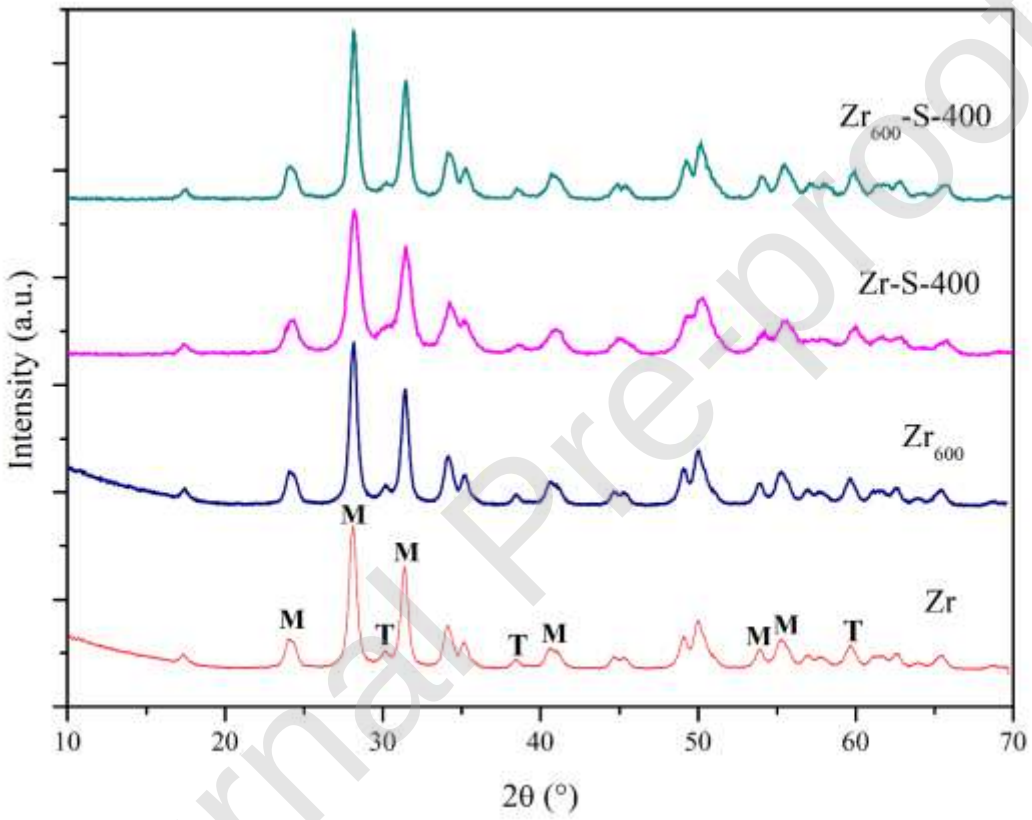

Figure 2: X-ray diffraction patterns of commercial zirconia and sulfate promoted zirconium oxides. **M**: monoclinic phase, **T**: tetragonal phase.

By means of potentiometric titration with n-butylamine, it is possible to estimate the strength and number of acid sites present in a solid. It is considered that the initial potential (E_0) indicates the maximum strength of the acid sites, and the value from which the plateau is reached is indicative of the total number of acid sites present in the titrated solid [53]. Potentiometric titration curves are shown in the Supplementary Information (Figure S2),

whereas the results are summarized in Table 2. It can be observed that all sulfated samples have higher acidity than the Zr and Zr_{600} samples and that an increase in the calcination temperature (from 400 to 600 °C) leads to a decrease in the number of acid sites in the sample. The latter behavior could be related to the loss of sulfate species at temperatures above 600 °C [54].

The superficial coverage of sulfate species was explored by XPS. The results of fresh Zr-S-400 and that reused in 4 runs show an S/Zr atomic ratio of 0.23 and 0.18, respectively (Figure S3). These values are similar, within the error of the technique, demonstrating the stability of the superficial sulfate species under the conditions studied.

An IR analysis of pyridine adsorbed on the Zr-S-400 sample was performed to determine the type of active site of the catalyst. For sulfated zirconia, traditional spectral interpretation attributes absorption peaks at 1607, 1574, and 1445 cm^{-1} to Lewis sites [55-57], 1490 cm^{-1} to Lewis and Brönsted sites [58], and 1640, 1610, and 1540 cm^{-1} to Brönsted acid sites [59]. Figure 3 shows the FTIR spectra of the Zr-S-400 sample. This spectrum produced peaks at 1445, 1490, 1540, 1574, 1610, and 1640 cm^{-1}, showing the presence of both Lewis and Brönsted acid sites in the material.

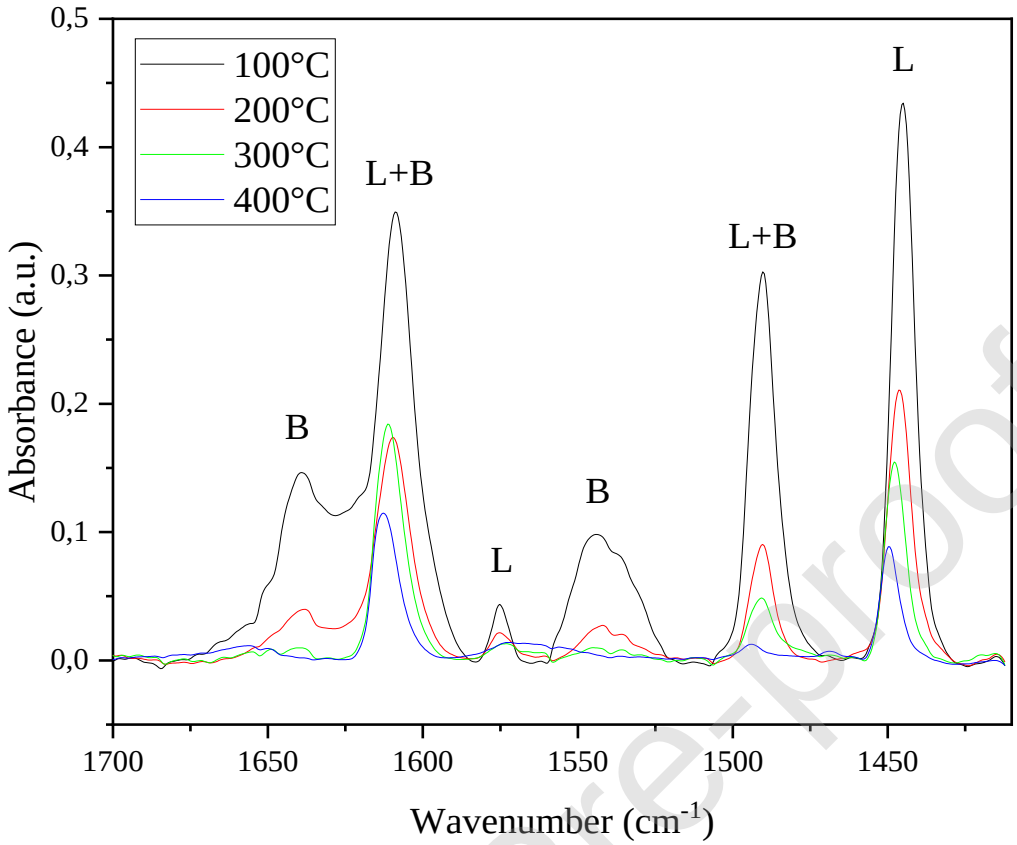

Figure 3: FTIR spectra of pyridine adsorbed on Zr-S-400 and evacuated at different temperatures. L = Lewis; B = Brönsted.

For comparison, the FTIR spectra of Zr is shown in the Supplementary Information (Figure S4). The concentrations of both sites were calculated from the intensities of the bands at 1540 cm^{-1} (B) and 1440 cm^{-1} (L), in the spectra obtained at different temperatures for each material (Table 3). It is observed that the sulfation process generates sites with Brönsted acidity and slightly increases the acidity of Lewis acid sites in Zr-S-400.

Table 3: Concentration (µmol.g^{-1}) of acid sites as calculated from adsorption/desorption of pyridine followed by IR absorption spectroscopy.

T (°C)	Concentration of acid sites (µmol.g^{-1})

	Zr		Zr-S-400	
	Lewis	Brönsted	Lewis	Brönsted
100	41	-	53	37
200	33	-	24	7
300	15	-	18	2
400	-	-	9	-

In view of the characterization results obtained, it is evident that the catalytic activity of the materials is linked to its acid properties. From the results shown in Table 1, the turnover frequency (TOF) of materials Zr-S-400, Zr-S-600 and Zr_{600}-S-400 were estimated as 66.3, 14.4 and 69.4 min^{-1}, respectively. Samples Zr-S-400 and Zr_{600}-S-400 have practically the same initial potential in the titration experiments (E_0 of 560 mV and 510 mV, respectively) indicating similar acid strength. This acid strength, which is due to the generation of new Brönsted acid sites in the sulfation process, is partially lost when the material is calcined at 600°C, leading to a decrease in the catalytic activity in sample Zr-S-600 [54].

3.3. Estimation of thermodynamic parameters

In order to determine the thermodynamic parameters, the reaction was carried out with the Zr-S-400 catalyst and in sufficient time to ensure no changes in the composition. Figure 4 presents the linearization of the experimental data. With these results, the dependence of the equilibrium constant with temperature could be expressed as $ln(K_{eq}) = 1397\frac{1}{T} - 6.304$.

The estimated values were ΔH^0 = -11.6 ± 1.1 kJ.mol^{-1}, and ΔG^0 = 4.0 ± 0.1 kJ.mol^{-1}, which show the exothermic nature of the reaction. Cornejo et al. [60] conducted a thermodynamic study considering an ideal behavior of the system and obtained a ΔH^0 = -6.6 ± 0.2 kJ.mol^{-1} and ΔG^0 = -0.4 ± 0.1 kJ.mol^{-1}. While their study predicts an exergonic character, ours predicts an endergonic character, highlighting the significance of considering the non-ideality of the reactive mixture in these studies.

Other studies have determined thermodynamic equilibrium parameters using ethanol as a solvent. Nanda et al. [44] determined a ΔH^0 = -30.1 ± 1.6 kJ.mol^{-1} and ΔG^0 = -2.1 ± 0.1 kJ.mol^{-1}, considering ideal behavior. Moreira et al. [45] estimated the thermodynamic

properties on the basis of activities, taking into account the non-ideal behavior of the mixture. The obtained values were ΔH^0 = -20.1 ± 1.1 kJ.mol^{-1} and ΔG^0 = 1.4 ± 0.1 kJ.mol^{-1}. Although the thermodynamic parameters of Moreira et al. could not be easily compared with our results, they also determined an endergonic character.

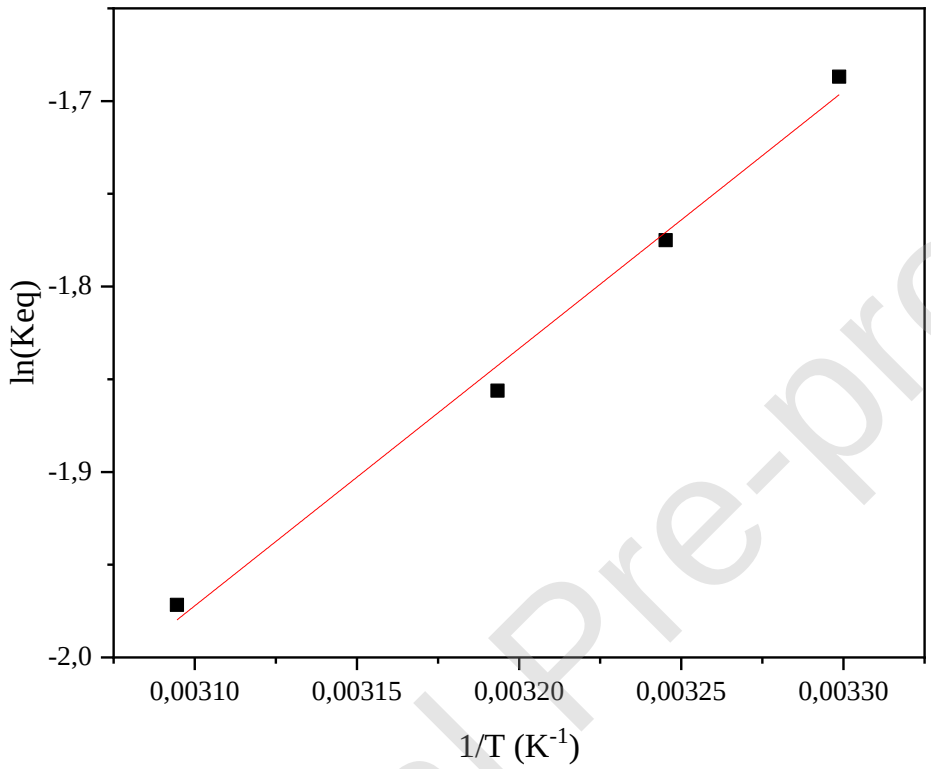

Figure 4: Linearization of ln (Keq) vs 1/T.

3.4 Reaction kinetic study

Kinetic model

To determine the kinetic model, the following reaction steps were taken:

Table 4: Steps involved in the kinetic model.

Step	Reaction
1	$Ac + * \leftrightarrow Ac^*$
2	$Gly + * \leftrightarrow Gly^*$
3	$Ac^* + Gly^* \leftrightarrow HA^* + *$
4	$HA^* + * \leftrightarrow Int^* + W^*$
5	$Int^* \leftrightarrow Solk^*$

6	$Solk^* \leftrightarrow Solk + *$
7	$W^* \leftrightarrow W + *$

The * symbol represents an active site of the catalyst, and the * superscript indicates that the component is adsorbed on the catalyst surface.

The reaction starts with the adsorption of both reactants on the catalyst surface. Then, a surface reaction between adsorbed glycerol (Gly*) and acetone (Ac*) leads to the formation of the hemiketal (3-(2-hydroxypropan-2-yloxy) propane-1,2-diol (HA^*). In step 4, a short-lived intermediate (Int^*) and water are formed, followed by a subsequent reaction, where the intramolecular reaction of the intermediate leads to the formation of Solketal ($Solk^*$). The final step of the reaction is the desorption of solketal and water from the catalyst surface.

In our reaction experiments with Zr-S-400, we did not detect the presence of the hemiketal even at low glycerol conversions. Using in situ Raman studies, Calvino-Casilda et al. detected the presence of an incipient formation of the hemiketal without a catalyst, and almost total selectivity to solketal in the presence of a catalyst [40]. Therefore, we consider that step 3 (formation of the hemiketal) is the controlling one.

The different equations employed (3-9) to develop the model are presented below:

$$K_1 = \frac{\theta_{Ac}}{\theta_V . a_{Ac}} \tag{3}$$

$$K_2 = \frac{\theta_{Gly}}{\theta_V . a_{Gly}} \tag{4}$$

$$r = K_3^+ \theta_{Ac} \theta_{Gly} - K_3^- \theta_{HA} \theta_V \tag{5}$$

$$K_4 = \frac{\theta_{Int} . \theta_W}{\theta_V . \theta_{HA}} \tag{6}$$

$$K_5 = \frac{\theta_{Solk}}{\theta_{Int}} \tag{7}$$

$$K_6 = \frac{\theta_V . a_{Solk}}{\theta_{Solk}} \tag{8}$$

$$K_7 = \frac{\theta_V . a_W}{\theta_W} \quad (9)$$

where θ represents the fraction of active sites occupied by each species and θ_V the free active sites. From equations 3 and 4, it is possible to obtain the following expression:

$$\theta_{Ac}\theta_{Gly} = K_1 . K_2 . a_{Ac} . a_{Gly}{\theta_V}^2 \quad (10)$$

From equations 6, 7, 8, and 9, the following expression for θ_{HA} is obtained:

$$\theta_{HA} = \frac{a_{Solk} . a_W . \theta_V}{K_4 . K_5 . K_6 . K_7} \quad (11)$$

Furthermore, taking into account the balance of active sites:

$$1 = \sum_{i=1}^{n} \theta_i \quad (12)$$

The reaction rate could be expressed from equations (3-12) as:

$$r = k \frac{a_{Gly} . a_{Ac} - \frac{a_{Solk} . a_W}{K_{eq}}}{(1 + \sum_{i=1}^{n} K_i . a_i)^2} \quad (13)$$

where k is the kinetic constant, K_i is the adsorption equilibrium constant of each component, and K_{eq} is the equilibrium constant of the reaction.

In the literature, several articles consider that water is the most strongly adsorbed component, and the adsorption of the remaining species could be neglected [44,45,61]. If we apply this consideration, the expression of the reaction rate is simplified to:

$$r = k \frac{a_{Gly} . a_{Ac} - \frac{a_{Solk} . a_W}{K_{eq}}}{(1 + K_W . a_W)^2} \quad (14)$$

It is well known that the adsorption of water on sulfated zirconia catalysts breaks the coordination of the Zr (IV) species bonded to sulfate species in order to bring Brönsted acid sites [62]. Therefore, the presence of water does not affect the number of active sites available, and the reaction rate could be further simplified to:

$$r = k \left(a_{Gly} . a_{Ac} - \frac{a_{Solk} . a_W}{K_{eq}} \right) \quad (15)$$

Estimation of kinetic parameters

The Mears criterion values were below 10^{-5}, and the Weisz-Prater criterion values below 10^{-8}, confirming that both external and internal diffusion limitations are negligible on the operation conditions. Temperature, acetone, and water concentration were varied systematically. Figure 5 shows the results of the kinetic model and the experimental ones. It is observed that the behavior at different temperatures is linked to the exothermic character of the reaction.

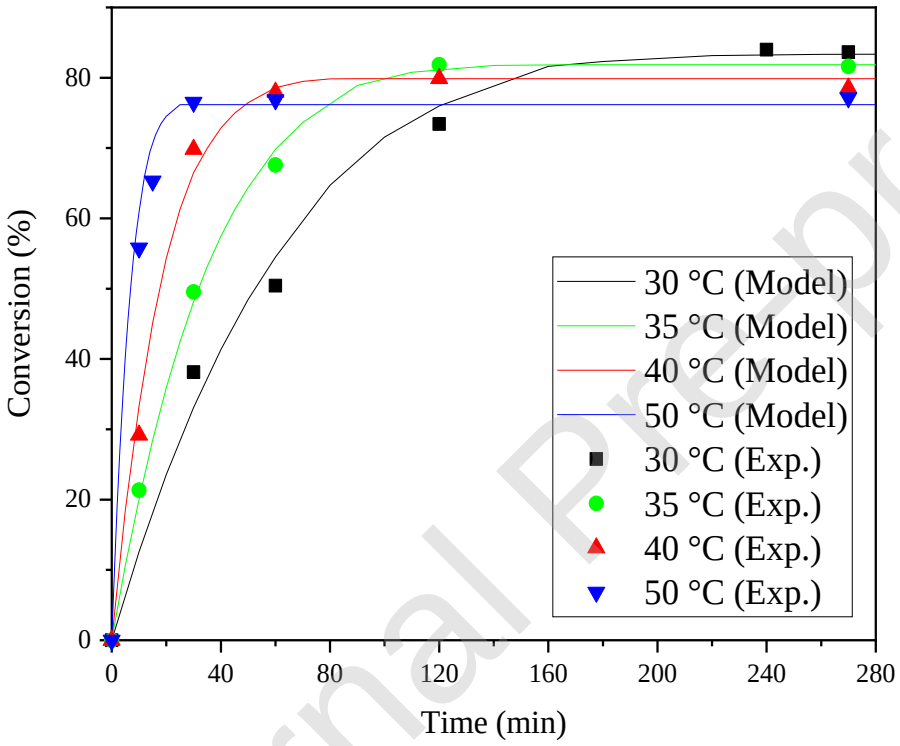

Figure 5: Effect of temperature on glycerol conversion. Experimental conditions: 0.2 MPa N_2, glycerol: acetone molar ratio = 1:6, 0.6 wt.% (catalyst: glycerol), Zr-S-400 catalyst.

Table 4 shows the estimated kinetic constant for each temperature. The estimation was performed by fitting the experimental data with the mathematical model (equation 15, Experimental Section). It is worth mentioning that these values were obtained assuming that none of the species is strongly adsorbed. To confirm this assumption, the experimental data were also adjusted considering water and solketal as strongly adsorbed species. Since

the kinetic parameters obtained were inconsistent, the consideration that none of the species involved are strongly adsorbed on the catalyst is acceptable.

Table 5: Estimated kinetic constant at different temperatures.

Temperature (°C)	k ($mol.g^{-1}.min^{-1}$)
30	0.04544 ± 0.0061
35	0.07126 ± 0.0079
40	0.11516 ± 0.0093
50	0.39720 ± 0.0460

From the results shown in Table 4, the activation energy value (Ea) was estimated as 88.1 ± 8.9 $kJ.mol^{-1}$, and the pre-exponential factor (k_0) as 6.55 x 10^{13} $mol.g^{-1}.min^{-1}$. These results are within the range of values obtained by other authors. Esteban et al. [61] estimated a value of Ea = 124.0 ± 12.9 $kJ.mol^{-1}$ assuming an Eley-Rideal mechanism on sulphonic ion-exchange resin in the absence of solvent. Nanda et al. [44] and Moreira et al. [45] reported Ea = 55.6 ± 3.1 $kJ.mol^{-1}$ and Ea = 69.0 ± 6.6 kJ/mol, respectively assuming an LHHW mechanism considering water as the most adsorbed species and using Amberlyst-35 and ethanol as a solvent. Rossa et al. [63] estimated an Ea = 44.8 ± 1.2 $kJ.mol^{-1}$ assuming a pseudo-homogeneous model and using an H-BEA zeolite. In the matter of homogeneous catalysis, da Silva et al. [64] and Ji et al. [65] reported the Ea of 26.0 $kJ.mol^{-1}$ using salt $Fe(NO_3)_3.9\ H_2O$ and the Ea of 28.2 $kJ.mol^{-1}$ using ionic liquid $[P(C_4H_9)_3C_{14}H_{29}][TsO]$, respectively.

Figures 6 A and B show the effect of the initial glycerol to acetone molar ratio on the kinetics and thermodynamics of the reaction. As shown in these figures, the increase in acetone concentration not only increases the conversion reached in the equilibrium but also

improves the reaction kinetics. This effect is more evident at lower catalyst content (Figure 6 B).

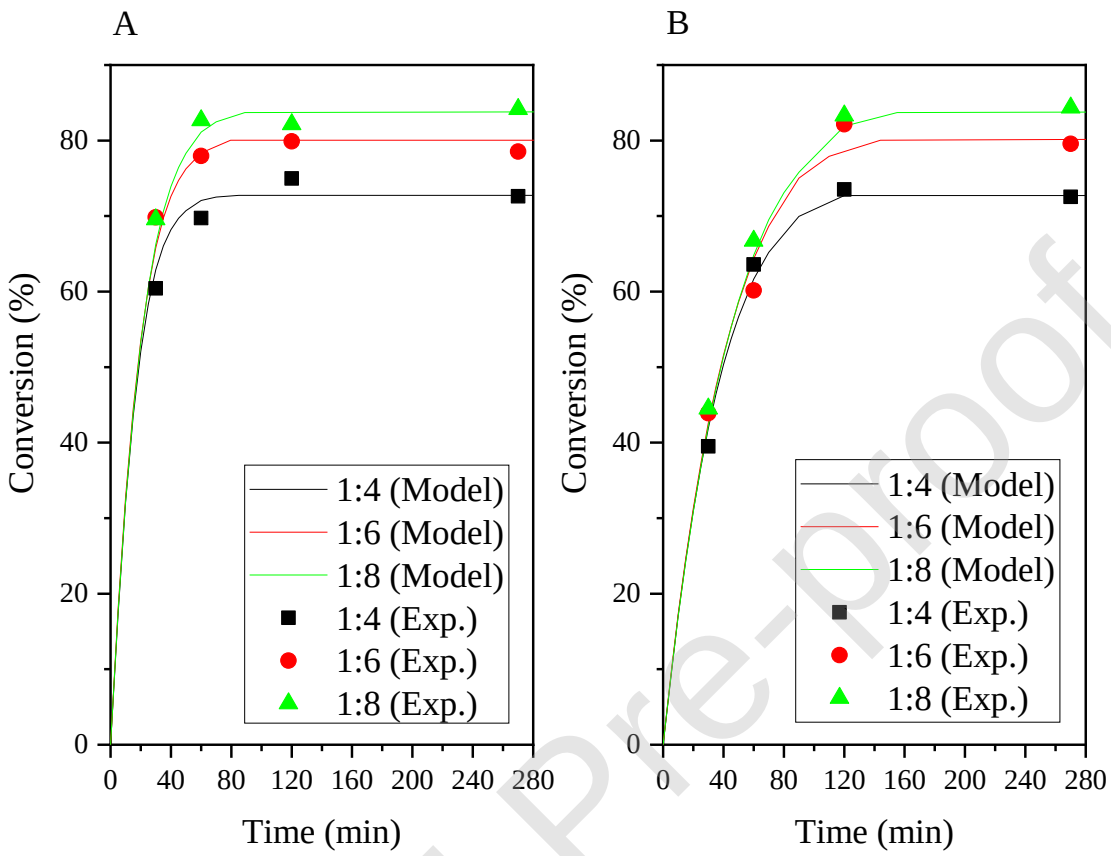

Figure 6: Effect of the glycerol to acetone molar ratio in the feed on glycerol conversion. Experimental conditions: 0.2 MPa N_2, 40 °C, Zr-S-400 catalyst. A: 0.6 wt.% (catalyst: glycerol); B: 0.3 wt.% (catalyst: glycerol).

Since one of the main impurities in the glycerol feedstock is the presence of water, it is essential to study the influence of this component on the reaction. In our study, water was added to the reaction mixture to simulate different glycerol feedstocks. Figure 7 shows the effect of water on the reaction rate at 5%, 10%, and 20% wt. of the total mass of glycerol. The presence of water in the reaction generates more extreme effects on the reaction rate and the conversion at equilibrium state. Feedstocks presenting 20% wt. of water significantly reduce the reaction rate, and the conversion at equilibrium decays from 80% to 63%. This highlights the need to use purified glycerol feedstock, with water concentration below 10% for better efficiencies in the chemical process.

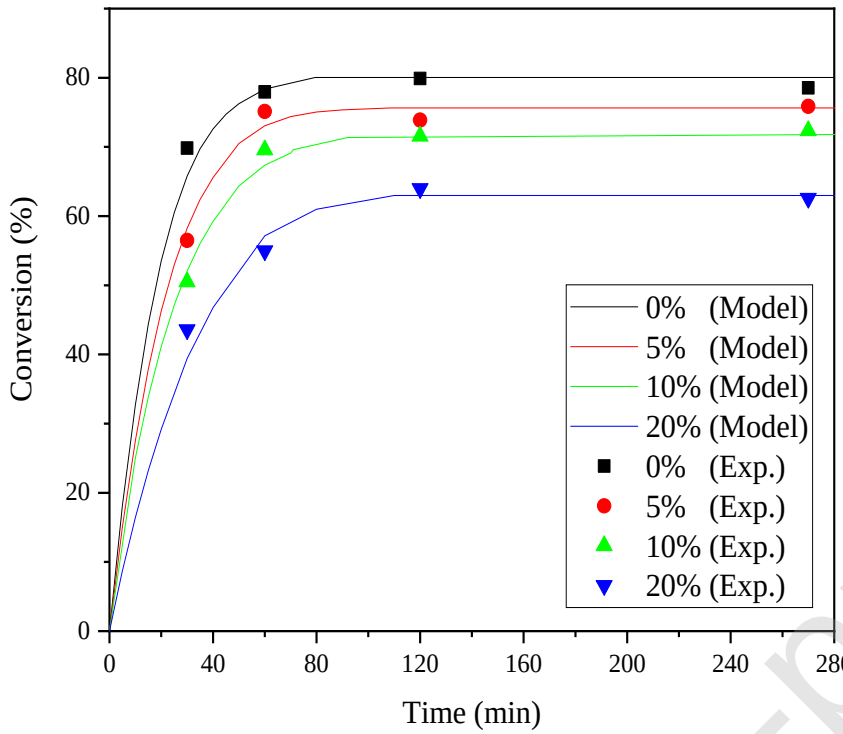

Figure 7: Effect of water composition in the feed on glycerol conversion. Experimental conditions: 0.2 MPa N_2, 40 °C, glycerol: acetone molar ratio = 1:6, 0.6 wt.% (catalyst: glycerol), Zr-S-400 catalyst.

4. Conclusions

The sulfation of a commercial zirconium oxide, by wet impregnation with a 0.5M H_2SO_4 solution, allowed us to obtain an active catalyst for the glycerol ketalization in the liquid phase. The characterization results showed a correlation between the calcination temperature and the acid sites generated on the materials. Among the catalysts studied, the Zr-S-400 material was the most active one and presented the largest acid density and greatest acid strength caused by the generation of new Brönsted sites, as determined by potentiometric titration and Pyridine FTIR. This catalyst exhibited a glycerol conversion of 80% in 1 hour of reaction at 40°C with a glycerol to acetone molar ratio = 1:6 and 0.6 wt% catalyst:glycerol.

The chemical equilibrium was analyzed using the UNIFAC method to determine the activity coefficients of each species. The thermodynamic parameters, standard enthalpy and

Gibbs free energies, were determined to be -11.6 ± 1.1 kJ.mol^{-1} and 4.0 ± 0.1 kJ.mol^{-1}, respectively.

Taking into account that the adsorption of water on this catalyst does not affect the number of acid sites available, a simple pseudo-homogeneous kinetic expression was developed and successfully adjusted to the experimental data in the range studied. Based on this model, the estimated activation energy of the reaction was 88.1 ± 8.9 kJ.mol^{-1}.

The study of the sensitivity of the reaction to the presence of water showed that the presence of water in the reactive mixture generates negative effects on the thermodynamics and kinetics of the reaction and, more importantly, it was determined that the concentration of water in the feedstock should be lower than 10% to keep the efficiency of the process.

Credit Author Statement

Julián A. Vannucci carried out all the experimental work, which was conceived and designed with Nora Nichio. Francisco Pompeo participated in the discussion of the results and the writing of the paper.

Declaration of interests

The authors declare that they have no known competing financial interests or personal relationships that could have appeared to influence the work reported in this paper.

Acknowledgments

This research work was possible due to the funds received from "Consejo Nacional de Investigaciones Científicas y Técnicas" (CONICET-PIP 0065), "Universidad Nacional de La Plata" (UNLP-I248). The doctoral fellowship granted by CONICET to Julian A. Vannucci is greatfully acknowledged.

References

[1] J. A. Melero, G. Vicente, G. Morales, M. Paniagua, J. Bustamante, Fuel, 89 (2010) 2011-2018.

[2] M. R. Nanda, Y. Zhang, Z. Yuan, W. Qin, H. S. Ghaziaskar, C. Xu, Renewable and Sustainable Energy Reviews, 56 (2016) 1022-1031.

[3] K. Fraatz, D. Mertin, I. Heep, US Patent 8231903B2, 2012.

[4] C. J. A. Mota, C. X. A. da Silva, N. Rosenbach Jr, J. Costa, F. da Silva, Energy Fuels, 24 (2010) 2733-2736.

[5] J. Esteban, A. J. Vorholt, A. Behr, M. Ladero, F. Garcia-Ochoa, Journal of Chemical & Engineering Data, 59 (2014) 2850-2855.

[6] J. Esteban, F. García-Ochoa, M. Ladero, Green Processing and Synthesis, 6 (2017) 79-89.

[7] P. Ferreira, I. M. Fonseca, A. M. Ramos, J. Vital, J. E. Castanheiro, Applied Catalysis B: Environmental, 98 (2010) 94-99.

[8] M. N. Timofeeva, V. N. Panchenko, V. V. Krupskaya, A. Gil, M. A. Vicente, Catalysis Communications, 90 (2017) 65-69.

[9] G. Vicente, J. A. Melero, G. Morales, M. Paniagua, E. Martín, Green Chemistry, 12 (2010) 899-907.

[10] L. Li, D. Cani, P. P. Pescarmona, Inorganica Chimica Acta, 431 (2015) 289-296.

[11] Z. Li, Z. Miao, X. Wang, J. Zhao, J. Zhou, W. Si, S. Zhuo, Fuel, 233 (2018) 377-387.

[12] H. Serafim, I. M. Fonseca, A. M. Ramos, J. Vital, J. Castanheiro, Chemical Engineering Journal, 178 (2011) 291-296.

[13] S. S. Priya, P. Selvakannan, K. V. Chary, M. L. Kantam, S. K. Bhargava, Molecular Catalysis, 434 (2017) 184-193.

[14] L. H. Vieira, L. G. Possato, T. F. Chaves, S. H. Pulcinelli, C. V. Santilli, L. Martins, Molecular Catalysis, 458 (2018) 161-170.

[15] X. Li, Y. Jiang, R. Zhou, Z. Hou, Applied Clay Science, 174 (2019) 120-126.

[16] Z. Miao, Z. Li, M. Liang, J. Meng, Y. Zhao, L. Xu, J. Mu, J. Zhou, S. Zhuo, W. Si, Chemical Engineering Journal, 381 (2020) 122594.

[17] X. Li, Y. Jiang, R. Zhou, Z. Hou, Applied Clay Science, 189 (2020) 105555.

[18] V. S. Marakatti, S. Marappa, E. M. Gaigneaux, New Journal of Chemistry, 43 (2019) 7733-7742.

[19] J. R. Sohn, D. H. Seo, Catalysis Today, 87 (2003) 219-226.

[20] A. I. Ahmed, S. A. El-Hakam, S. E. Samra, A. A. EL-Khouly, A. S. Khder, Colloids and Surfaces A: Physicochemical and Engineering Aspects, 317 (2008) 62-70.

[21] A. Corma, M. I. Juan-Rajadell, J. M. López-Nieto, A. Martinez, C. Martínez, Applied Catalysis A: General, 111 (1994) 175-189.

[22] X. Li, K. Nagaoka, J. A. Lercher, Journal of Catalysis, 227 (2004) 130-137.

[23] N. Essayem, Y. Ben Taârit, C. Feche, P. Y. Gayraud, G. Sapaly, C. Naccache, Journal of Catalysis, 219 (2003) 97-106.

[24] A. Corma, J. M. Serra, A. Chica, Catalysis Today, 81 (2003) 495-506.

[25] A. Wolfson, O. Shokin, D. Tavor, Journal of Molecular Catalysis A: Chemical, 226 (2005) 69-76.

[26] H. Nagai, K. Kawahara, S. Matsumura, K. Toshima, Tetrahedron Letters, 42 (2001) 4159-4162.

[27] P. S. Reddy, P. Sudarsanam, B. Mallesham, G. Raju, B. M. Reddy, Journal of Industrial and Engineering Chemistry, 17 (2011) 377-381.

[28] V. T. Vasantha, N. J. Venkatesha, S. Z. M. Shamshuddin, J. Q. D'Souza, B. G. V. Reddy, ChemistrySelect, 3 (2018) 602-608.

[29] M. R. Nanda, Z. Yuan, W. Qin, H. S. Ghaziaskar, M. A. Poirier and C. Xu, Applied Energy, 123 (2014) 75-81.

[30] S. Brunauer, P. H. Emmett, E. Teller, Journal of the American Chemical Society, 60 (1938) 309-319.

[31] E. P. Barrett, L. G. Joyner, P. P. Halenda, Journal of the American Chemical Society, 73 (1951) 373-380.

[32] C. Emeis, Journal of Catalysis, 141 (1993) 347-354.

[33] L. Roldán, R. Mallada, J. M. Fraile, J. A. Mayoral, M. Menéndez, Asia-Pacific Journal of Chemical Engineering, 4 (2009) 279-284.

[34] O. Ilgen, S. Yerlikaya, F. O. Akyurek, Periodica polytechnica chemical engineering, 61 (2017) 144-148.

[35] S. Sandesh, A. B. Halgeri, G. V. Shanbhag, Journal of Molecular Catalysis A: Chemical, 401 (2015) 73-80.

[36] S. Zhang, S. Zhao, Y. Ao, Applied Catalysis A: General, 496 (2015) 32-39.

[37] P. Manjunathan, S. P. Maradur, A. B. Halgeri, G. V. Shanbhag, Journal of Molecular Catalysis A: Chemical, 396 (2015) 47-54.

[38] J. Kowalska-Kus, A. Held, M. Frankowski, K. Nowinska, Journal of Molecular Catalysis A: Chemical, 426 (2017) 205-212.

[39] A. Fredenslund, J. Gmehling, P. Rasmussen, Vapor-liquid Equilibria Using Unifac: A Group-Contribution Method, Elsevier, 1977.

[40] V. Calvino-Casilda, K. Stawicka, M. Trejda, M. Ziolek, M. A. Bañares, The Journal of Physical Chemistry, 118 (2014) 10780-10791.

[41] B. Mallesham, P. Sudarsanam, G. Raju, B. M. Reddy, Green Chemistry, 15 (2013) 478-489.

[42] L. Li, T. I. Korányi, B. F. Sels, P. P. Pescarmona, Green Chemistry, 14 (2012) 1611-1619.

[43] L. P. Ozorio, R. Pianzolli, M. B. S. Mota, C. J. A. Mota, Journal of the Brazilian Chemical Society, 23 (2012) 931-937.

[44] M. R. Nanda, Z. Yuan, W. Qin, H. S. Ghaziaskar, M. A. Poirier, C. C. Xu, Fuel, 117 (2014) 470-477.

[45] M. N. Moreira, R. P. V. Faria, A. M. Ribeiro, A. E. Rodrigues, Industrial & Engineering Chemistry Research, 58 (2019) 17746-17759.

[46] E. G. Scheibel, Industrial & Engineering Chemistry, 46 (1954) 1569-1579.

[47] L. R. Perkins, C. J. Geankoplis, Chemical Engineering Science, 24 (1969) 1035-1042.

[48] A. W. Hixson, S. J. Baum, Industrial & Engineering Chemistry, 33 (1941) 478-485.

[49] A. Feliczak-Guzik, I. Nowak, Microporous and Mesoporous Materials, 277 (2019) 301-308.

[50] I. S. Gomes, D. C. de Carvalho, A. C. Oliveira, E. Rodríguez-Castellón, S. Tehuacanero-Cuapa, P. T. C. Freire, J. M. Filho, G. D. Saraiva, F. F. de Sousa, R. Lang, Chemical Engineering Journal, 334 (2018) 1927-1942.

[51] A. L. G. Pinheiro, J. V. C. do Carmo, D. C. Carvalho, A. C. Oliveira, E. Rodríguez-Castellón, S. Tehuacanero-Cuapa, L. Otubo, R. Lang, Fuel Processing Technology, 184 (2019) 45-56.

[52] D. C. de Carvalho, A. C. Oliveira, O. P. Ferreira, J. M. Filho, S. Tehuacanero-Cuapa, A. C. Oliveira, Chemical Engineering Journal, 313 (2017) 1454-1467.

[53] L. R. Pizzio, M. N. Blanco, Microporous and Mesoporous Materials, 103 (2007) 40-47.

[54] G. X. Yan, A. Wang, I. E. Wachs, J. Baltrusaitis, Applied Catalysis A, General, 572 (2019) 210-225.

[55] B. T. Loveless, A. Gyanani, D. S. Muggli, Applied Catalysis B: Environmental, 84 (2008) 591-597.

[56] C. D. Miranda M., A. E. Ramírez S., S. G. Jurado, C. R. Vera, Journal of Molecular Catalysis A: Chemical, 398 (2015) 325-335.

[57] C. Breitkopf, S. Matysik, H. Papp, Applied Catalysis A: General, 301 (2006) 1-8.

[58] W. H. Chen, H. H. Ko, A. Sakthivel, S. J. Huang, S. H. Liu, A. Y. Lo, T. C. Tsai, S. B. Liu, Catalysis Today, 116 (2006) 111-120.

[59] K. T. Wan, C. B. Khouw, M. E. Davis, Journal of Catalysis, 158 (1996) 311-326.

[60] A. Cornejo, M. Campoy, I. Barrio, B. Navarrete, J. Lázaro, Reaction Chemistry & Engineering, 4 (2019) 1803-1813.

[61] J. Esteban, M. Ladero, F. García-Ochoa, Chemical Engineering Journal, 269 (2015) 194-202.

[62] M. Hino, M. Kurashige, H. Matsuhashi, K. Arata, Thermochimica Acta, 441 (2006) 35-41.

[63] V. Rossa, Y. S. P. Pessanha, G. C. Díaz, L. D. T. Câmara, S. B. C. Pergher, D. A. G. Aranda, Industrial & Engineering Chemistry Research, 56 (2017) 479-488.

[64] M. J. da Silva, A. A. Rodrigues, P. F. Pinheiro, Fuel, 276 (2020) 118164.

[65] Y. Ji, T. Zhang, X. Gui, H. Shi, Z. Yun, Chinese Journal of Chemical Engineering, 28 (2020) 158-164.